RSC Advances

ROYAL SOCIETY
OF **CHEMISTRY**

www.rsc.org/advances

Journal Name

Dynamic Article Links ▶

ARTICLE TYPE

Synthesis of magnetic porous γ-Fe₂O₃/C@HKUST-1 composites for efficient removal of dyes and heavy metal ions from aqueous solution

Yuhao Xiong, Fanggui Ye,* Cong Zhang, Shufen Shen, Linjing Su, Shulin Zhao

A novel and inexpensive approach was adopted to develop magnetic porous γ-Fe₂O₃/C@HKUST-1 composites for the adsorption of dye and heavy metal ions from aqueous solution. The γ-Fe₂O₃/C with unique functional groups present such as −OH and −NH₂ was used as the support to directly grow HKUST-1 by a stepwise liquid-phase epitaxy process. The crystallographic, morphology, and magnetic

10 properties as well as porosity of the as-synthesized γ-Fe₂O₃/C @HKUST-1 composites were carefully studied by XRD, SEM, TEM, XPS, TGA, and BET. Results indicated that the BET surface area, micropore volume, and saturation magnetization of the γ-Fe₂O₃/C @HKUST-1 are 993.4 m² g⁻¹, 0.69 cm³ g⁻¹, and 12.6 emu g⁻¹, respectively. In addition, a uniform distribution of ultrafine γ-Fe₂O₃ nanoparticles with an average diameter of 2–3 nm was observed in the γ-Fe₂O₃/C@HKUST-1 composites. Our results

15 showed that methylene blue (MB) and Cr(VI) (used as a model for typical dye pollutants and heavy metal iron) are effectively removed from aqueous solutions by γ-Fe₂O₃/C@HKUST-1. The maximum adsorption capacities were 370.2 and 101.4 mg g⁻¹ of adsorbent for MB and Cr(VI), respectively. Moreover, a removal efficiency of about 90% was retained after five cycles of consecutive adsorption-desorption. The adsorption kinetics data were well described by a pseudo-second-order model ($R^2 > 0.99$),

20 and equilibrium data were well fitted to the Langmuir isotherm model ($R^2 > 0.99$). Finally, our results suggested that the γ-Fe₂O₃/C@HKUST-1 composites have a great potential to be employed for treatment of wastewater containing MB and Cr(VI).

Introduction

In recent years, water pollution has become a major issue, as a
25 large amount of industrial pollutants is found to cause serious adverse health effects on humans, hindering the development of social economy; of particular concern is water pollution caused by heavy metal ions and dyes.[1] For example, millions of tons of dye wastewater are discharged from different sources, including
30 plastic, textile, leather, cosmetics, paper-making, printing, and dye-manufacturing industries.[2] Furthermore, water contamination of heavy metal ions is severe, as Cr(VI), discharged from stainless steel, electroplating, metal finishing, and leather tanning, is considered as a human genotoxic carcinogen that can be easily
35 absorbed into the body through the digestive system, respiratory tract, and skin.[3] For this reason, development of effective technologies to remediation of toxic pollutants from aqueous solutions is important for the protection of public health and social economy.
40 Various methods have been developed to remove dyes and heavy metal ions from aqueous solution, including photodegradation,[4] chemical precipitation,[5] and adsorption.[6,7] Among these, absorption is the most versatile and effective method, because the pollutants are not only moderately stable to
45 light and heat, but also resistant to oxidation and biodegradation.[8]

In addition, regeneration, low costs, and relatively simple operation make absorption the technique of choice.[9] In the past decades, several effective adsorbents have been developed using chitosan,[10] carbon materials,[11, 12] resins,[13] and other materials.[14, 15]
50 Due to their low cost, widespread source, and stability to acids or bases, carbon materials have received great attention.[16] This type of adsorbent shows a high-adsorption capacity (e.g., 539.53 mg/g for Cr(VI))[6], but requires a tedious high-speed centrifugation or filtration separation after adsorption. One of the most effective
55 strategies to overcome these problems is the preparation of magnetic carbon-based composites,[17, 18] which can be effectively separated under an external magnetic field and recycled for reuse. For instance, Zhu *et al*. have selected hydrochar as a carbon precursor to prepare magnetic carbon composites for malachite
60 green removal.[19] Zhou and co-workers employed polystyrene microspheres and Fe²⁺ to fabricate magnetic porous-carbon spheres to remove methylene blue (MB).[20] Torad *et al*. reported magnetic carbon material loaded with magnetic cobalt nanoparticles using ZIF-67 as template for water treatment.[21] It
65 has been demonstrated that magnetic carbon composites have great potential for water treatment. However, the conditions of synthesis of the as-reported magnetic carbon-based composites are usually harsh (under inert atmosphere and about 800 □).

Metal-organic framework (MOF)—a new type of functional
70 materials have attracted much attention in the field of water

treatment, owing to their large surface areas, high chemical and thermal stability, unsaturated metal sites, and tunable surface properties.[22] Interestingly, the high specific surface area of MOF combined with carbon materials can improve the adsorption performance. For example, MOF/graphite oxide composites greatly increase the surface area and the adsorption capacity of MB.[23] The research groups of Lu and Somani have also demonstrated that carbons/MOF hybrids can enhance gas capture capability.[24, 25] Inspired by the fact that carbon/MOF composites can increase the adsorption capacity and that magnetic carbon composites can be magnetically separable and reusable, we proposed a method for wastewater treatment with magnetic carbon/MOF composites. To the best of our knowledge, few studies about the removal of pollutants from the aqueous solution by using magnetic carbon/MOF composite have been reported. For instance, Hu *et al*. reported that magnetic hybrid Fe_3O_4/MOF/graphene oxides have a good recycle for dyeing wastewater treatment.[26] However, the adsorption capacity of this composite is limited (about 180 mg g^{-1}). Thus, studies on novel carbon/MOF magnetic adsorbents with improved adsorption performance are highly desireable.

In the present work, we describe the synthesis of a highly porous magnetic γ-Fe_2O_3/C@HKUST-1 composite carried out via two facile steps; its application for an efficient adsorption of pollutants from aqueous solution is also discussed. First, magnetic porous γ-Fe_2O_3/C was simply and rapidly (3 min) synthesized by a microwave-enhanced high-temperature ionothermal method from starch, which is nontoxic, inexpensive, naturally abundant, and environmentally friendly. Next, HUKST-1 was grown onto the γ-Fe_2O_3/C particles using liquid-phase epitaxy without chemical modification. The prepared γ-Fe_2O_3/C@HKUST-1 composites was fully characterized. The adsorption kinetics, isotherms and adsorption mechanism of γ-Fe_2O_3/C@HKUST-1 were fully investigated using MB and Cr (VI) as model pollutants.

Experimental

Materials and Chemicals

All chemicals were at least of analytical reagent grade and used without further purification. $FeCl_3 \cdot 6H_2O$ was purchased from Aladdin (Shanghai, China). Starch was purchased from Wuzhou Saojiao Food Co., Ltd. (Guangxi, China). $Cu(Ac)_2$, 1,3,5-benzenetricarboxylic acid (H_3btc), anhydrous ethanol, MB, $K_2Cr_2O_7$, and activated carbon were purchased from Shanghai Chemical Reagents Corporation (Shanghai, China). MB and Cr(VI) stock solutions of 1000 mg L^{-1} were prepared and further diluted to the required concentrations for testing the adsorption capacity and investigating the adsorption process. Ultrapure water was produced by a Millipore purification system (Bedford, MA, USA) and used to prepare all aqueous solutions.

Synthesis of magnetic porous γ-Fe_2O_3/C

The magnetic porous γ-Fe_2O_3/C materials were synthesized using $FeCl_3 \cdot 6H_2O$ and starch as precursors. In particular, 5.0 g starch was dissolved in 45 mL ultrapure water at room temperature with magnetic stirring for 30 min until the starch was fully dissolved. A weight of 4.0 g $FeCl_3 \cdot 6H_2O$ was added into the starch solution and continue stirring for 24 h at 60 ℃ to obtain a uniform yellow colloidal mixture , then reacted in a microwave reactor (Glanz WD800BL23, Shenzhen, China) with 600 W microwave powers for 3 min, and finally dried in an oven at 80 ℃ for 24 h. The obtained solid was ground in a glass mortar to obtain a very fine powder. Subsequently, 3.0 g of powders and 9.0 g $ZnCl_2$ were well mixed, followed by reaction in a microwave reactor with 600 W microwave powers for 3 min. The obtained black γ-Fe_2O_3/C composites were washed five times with diluted HCl (0.01 mol L^{-1}, 100 mL) and ultrapure water. These were then separated by an external magnetic field from aqueous solutions, and finally dried at 100 ℃ in *vacuo*.

Synthesis of magnetic porous γ-Fe_2O_3/C@HKUST-1

The synthesis of HKUST-1 nanoparticles on pretreated γ-Fe_2O_3/C was conducted using the stepwise liquid-phase epitaxy process introduced by Silvestre *et al*. with some modifications.[27] In particular, 10 mL of 10 mM $Cu(Ac)_2$ ethanol solution and 10 mL of 10 mM of H_3btc in ethanol were alternately added to 0.1 g γ-Fe_2O_3/C. In both cases, the suspension was kept for 10 min under shaking, which guarantees complete mixing and fast mass transfer at the solid-liquid interface. The samples were recovered by an external magnetic field and washed three times with ethanol. After twenty cycles, the samples were washed with ethanol, and dried under *vacuum* at 80 ℃ . Synthesis of γ-Fe_2O_3/C@HKUST-1 is depicted in Scheme 1.
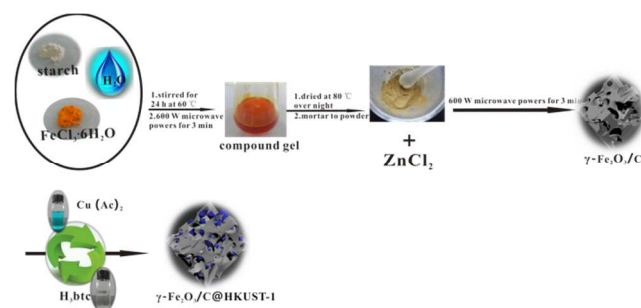
Scheme 1 Synthesis of γ-Fe_2O_3/C@HKUST-1.

Synthesis of HKUST-1

HKUST-1 was synthesized according to a modified method previously reported.[28] H_3btc (250 mg) was added to 40 mL of ethanol solution. $Cu(Ac)_2$ (430 mg) was dissolved in 20 mL water. The two solutions were mixed with stirring. Triethylamine (0.25 mL) was added to the mixture and then stirred for 3 h. The product was collected by filtration, washed with ethanol, and finally dried.

Characterization of γ-Fe_2O_3/C@HKUST-1

X-ray diffraction (XRD) patterns of the samples were recorded on a D/max 2550 VB/PC diffractometer (Rigaku, Japan) with Cu Kα radiation (λ=0.15418 nm). X-ray photoelectron spectroscopy (XPS) data were obtained with a Thermo ESCALAB 250XI electron spectrometer (Thermo, USA) using 150 W Al Kα radiation. Fourier transform infrared (FT-IR) spectra (4000–400 cm^{-1}) in KBr were recorded using a PE Spectrum One FT-IR spectrometer (PE, USA). The morphologies and microstructures of as-synthesized samples were characterized by field-emission scanning electron microscopy (SEM) (NoVaTM Nano SEM 430,

FEI, USA) and transmission electron microscopy (TEM) (Tecnai G20, FEI, USA). The specific surface areas of the as-synthesized samples were calculated by Brunauer-Emmett-Teller (BET). Nitrogen adsorption and desorption at 77 K using an adsorption instrument (3Flex, Micromeritics, USA) to evaluate the pore structures, pore size distributions and pore volumes were analyzed by the Barrett-Joyner-Halenda (BJH). The magnetization curves were measured at 300 K under a magnetic field (in the range of −20 and 20 kOe) on a MPMS-XL-7 magnetometer (Quantum Design, USA). Surface elements of samples were mapped with electron dispersive spectroscopy (EDS) equipped with SEM. Raman spectra were performed on an inVia spectrometer (Renishaw, UK) with He–Ne laser operating at a wavelength of 514 nm; the curve fitting was performed with a combination of Gaussian line shapes that gave the minimum fitting error. Thermogravimetric analysis (TGA) was performed with a LABSYS evo TG-DSC/DTA instrument (Setaram Instrumentation, France) under air at a heating rate of 20 ℃ min^{-1}.

Adsorption experiments

The adsorption experiments were carried out in a water bath at a constant temperature of 30 ℃. Both the heavy metal ion (Cr(VI)) and organic pollutant (MB) were employed as pollutants in water for the adsorption measurements. As for the adsorption of the heavy metal ion, 5 mL of Cr(VI) aqueous solutions with different initial concentrations were dispersed with 10.0 mg of the adsorbents. After a certain period of adsorbing time and magnetic separation using a permanent magnet, the remaining Cr(VI) concentrations of the solutions were determined with the 1,5-diphenylcarbazide method.[29] To explore the effect of pH, HCl and NaOH solutions were used to obtain a pH in the range of 3.0 and 9.0. For the adsorption of organic pollutants, the adsorbent (10.0 mg) was added to the aqueous solutions of MB (5 mL) with different concentrations at a constant temperature of 30 °C under dark conditions. Once the equilibrium was reached, the adsorbents were magnetically separated using a magnet, and the equilibrium concentration of MB was determined using a UV-Vis spectrophotometer (Cary 60, Agilent, USA) at the calibrated maximum wavelength of 665 nm. The adsorption capacity at equilibrium (q_e, mg/g) was calculated according to the following equation:

$$q_e = \frac{(C_0 - C_e)\, V}{m} \qquad (1)$$

where C_0 (mg L^{-1}) and C_e (mg L^{-1}) are the initial and equilibrated concentrations, respectively, V(L) is the volume of the solution and m (g) is the weight of the adsorbent used.

Results and discussion

Synthesis and characterization of γ-Fe$_2$O$_3$/C@HKUST-1

As illustrated in Scheme 1, the abundant –OH groups in starch showed strong interactions with Fe^{3+}, favoring the adsorption of the Fe^{3+} ion; after stirring for 24 h, this led to the formation of a starch-Fe precursor. Fe^{3+} was hydrolyzed to Fe hydroxides (*e.g.*, FeO(OH)) in the microwave-reactor heating process. A very fine powder was then obtained after drying and grinding.

Subsequently, ZnCl$_2$ was chosen as the microwave heating medium for fine powder carbonization to form magnetic porous γ-Fe$_2$O$_3$/C with unique functional groups present such as –OH and −NH$_2$. Finally, HKUST-1 was directly grown on the surface of γ-Fe$_2$O$_3$/C via a stepwise liquid-phase epitaxy.

In order to determine the crystalline structures of the synthesized samples, these were analyzed by a powder XRD technique (Fig. 1). The main characteristic peaks of γ-Fe$_2$O$_3$ appeared around 30.12°, 35.34°, 43.06°, 53.32°, 56.80°, and 62.46°, which correspond to (111), (220), (311), (400), (422), (511), and (440) planes, respectively.[30]
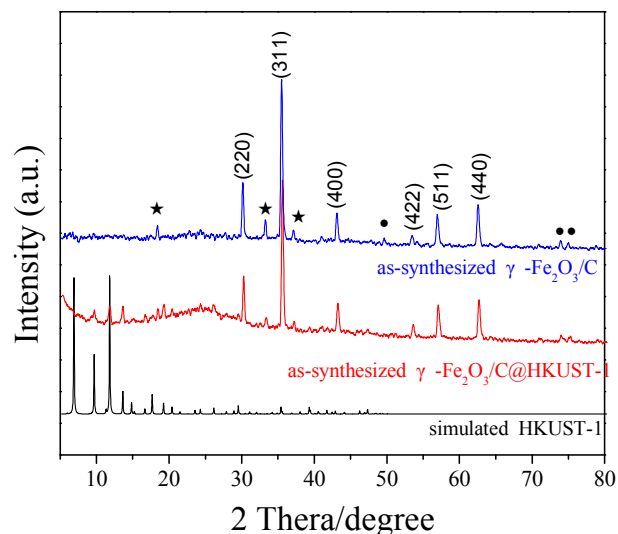
The observed diffraction peaks well matched with the standard diffraction peaks (JCPDS file 39-1346). In addition to the characteristic peaks of γ-Fe$_2$O$_3$, other peaks (marked with "★"and "●") appear in the XRD patterns; these can be indexed to the spinel lattice of ZnO and ZnCl$_2$. This finding indicates that these species cannot be completed removed by washing with 0.01 M HCl.[31] According to previous work,[24] due to the presence of amorphous carbon matrix, the XRD pattern of the γ-Fe$_2$O$_3$/C@HKUST-1 composite displays certain weakening of the diffraction intensity compared with the pure HKUST-1. But we notice that the reflection peaks (7.5°-30°) of the γ-Fe$_2$O$_3$/C@HKUST-1 composite match well with the simulated HKUST-1. In order to make clear of reflection peaks (7.5°-30°) match well with the simulated HKUST-1, local amplification figure has been drawn (Fig. S1). Result confirming that the structure of HKUST-1 is preserved.

The identification of the exact nature of the oxide phase based solely on the XRD is non-trivial, because Fe$_3$O$_4$ also exhibits similar peaks. In order to clearly distinguish the γ-Fe$_2$O$_3$ and Fe$_3$O$_4$ phases, XPS measurements are necessary. The survey spectrum of γ-Fe$_2$O$_3$/C@HKUST-1 (Fig. S2) shows the presence of two sharp peaks located at 284.7 and 532.3 eV, which were assigned to C 1s and O 1s binding energies of the composite,[32, 33] respectively; this implies that the main species are C and O.

Moreover, the peaks at 711.5 and 935.1 eV correspond to Fe 2p and Cu 2p of the γ-Fe_2O_3 and HKUST-1 particles. As the high-resolution spectrum of Fe (Fig. S3) shows, the binding energies of 711.3 and 724.8 eV correspond to Fe $2p_{3/2}$ and Fe $2p_{1/2}$ of Fe^{3+}
5 contained in γ-Fe_2O_3. In addition, the characteristic satellite peaks of Fe^{3+} species were observed but Fe^{2+} species were absent, suggesting the absence of Fe_3O_4 in the composites.[30, 31] Therefore, we can infer that the oxide phase is γ-Fe_2O_3.

The functional groups of the surfaces of γ-Fe_2O_3/C, γ-
10 Fe_2O_3/C@HKUST-1, and HKUST-1 were investigated by FT-IR spectra (Fig. S4); the characteristic peak at 3420 cm^{-1} is typical of an O−H bond and N−H bond stretching; the peaks at 2915 cm^{-1} can be assigned to ν (CH_2) in the CH_2OH group and ν (C−H) in the pyranose ring.[10] Between 1700 and 1290 cm^{-1}, the spectra
15 of HKUST-1 and γ-Fe_2O_3/C@HKUST-1 show similar features. The asymmetric stretching of the carboxylate groups in H_3btc is detected at 1700–1560 cm^{-1}, and the symmetric stretching of the carboxylate groups in H_3btc is observed at 1376 and 1440 cm^{-1}. The peaks at 750 and 590 cm^{-1} correspond to the out-of-plane
20 vibrations of H_3btc and Fe–O vibrations, respectively.[23, 24]

The structure of the carbon phase of γ-Fe_2O_3/C@HKUST-1 was also studied by Raman spectroscopy. As shown in Fig. S5, two broad peaks displaying at about 1354 and 1593 cm^{-1}, which were assigned to the defect sp^3 carbon band (D band) and stretching
25 vibrations of basal graphite layers (G band), respectively.[19, 34] Moreover, the D-band and G-band exhibited similar intensities (I_G/I_D=0.94), indicating the amorphous carbon structure of this sample.[20]

Fig. 2 shows the TGA curves of γ-Fe_2O_3/C@HKUST-1 and γ-
30 Fe_2O_3/C obtained under air; the former showed a three step weight loss. The first main weight-loss stage was due to the dehydration of the material up to 130 °C. The calculated water content of γ-Fe_2O_3/C@HKUST-1 and γ-Fe_2O_3/C is 8.3% and 4.8%, respectively.

35
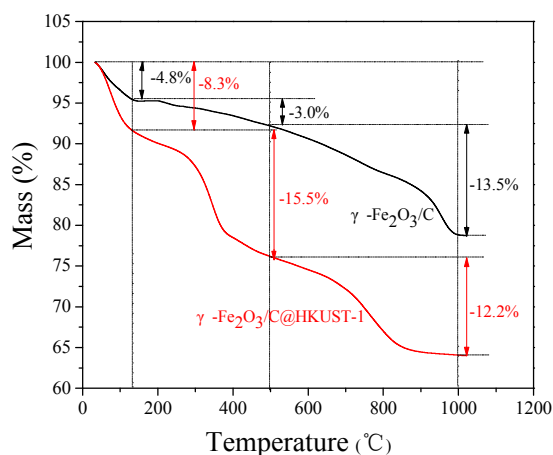
Fig. 2 TGA curves of γ-Fe_2O_3/C@HKUST-1 and γ-Fe_2O_3/C.

With HKUST-1 being hydrophilic in nature, an increase in the water content in the composite materials was observed as amount of HKUST-1 loading. As reported previously,[35] the HKUST-1
40 framework is stable up to 300 °C; therefore, the second weight loss observed between 130 and 500 °C mainly indicates the decomposition of HKUST-1. After 500 °C, the weight loss of γ-

Fe_2O_3/C@HKUST-1 and γ-Fe_2O_3/C is similar, suggesting that the carbon of composite is decomposed into CO_2.
45 The magnetization of γ-Fe_2O_3/C and γ-Fe_2O_3/C@HKUST-1 was investigated by MPMS measurements (Fig. 3), saturation magnetization (Ms) values of γ-Fe_2O_3/C@HKUST-1 and γ-Fe_2O_3/C particles being 12.6 and 18.8 emu g^{-1}, respectively.
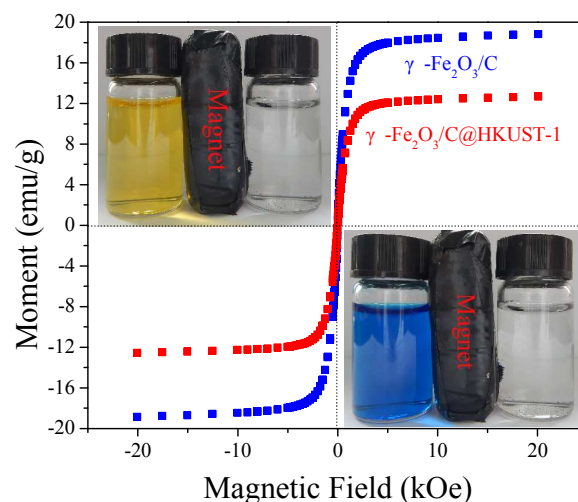
50 **Fig. 3** Magnetization curves of γ-Fe_2O_3/C@HKUST-1 and γ-Fe_2O_3/C at 300 K; inset: separation of the samples from solution under an external magnetic field.

Notably, after successfully loading HKUST-1, the Ms values of γ-Fe_2O_3/C decreased 6.2 emu g^{-1}. In spite of that, the magnetic
55 susceptibility of the final γ-Fe_2O_3/C@HKUST-1 is sufficiently strong to facilitate a rapid separation of the adsorbent (within 20 s) from solution using an external magnet field.

The N_2 adsorption-desorption isotherms of γ-Fe_2O_3/C @HKUST-1 and γ-Fe_2O_3/C are shown in Fig. 4. These data
60 suggest that both materials exhibit typeⅡisotherms with an H4 hysteresis loop, demonstrating that microporosity and mesoporosity coexist in these materials.[17, 24] The N_2 uptake of γ-Fe_2O_3/C@HKUST-1 was found to be higher than that of the original γ-Fe_2O_3/C; the BET surface areas of γ-
65 Fe_2O_3/C@HKUST-1 and γ-Fe_2O_3/C were 993.4 and 861.6 m^2 g^{-1}, respectively (Table 1). This indicates that the growth of HKUST-1 may lead to an increase in the surface areas of γ-Fe_2O_3/C.
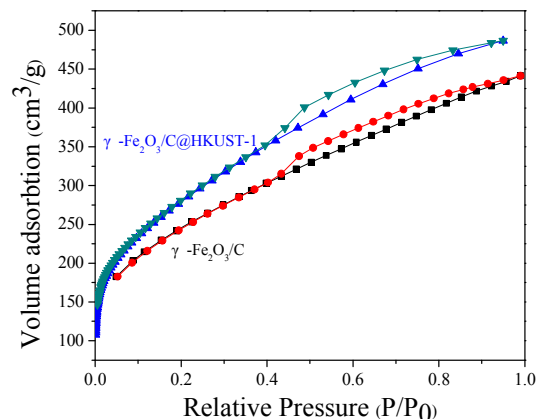
Fig. 4 N_2 adsorption–desorption isotherm of γ-Fe_2O_3/C@HKUST-1 and
70 γ-Fe_2O_3/C.

Table 1 The porosity analysis of γ-Fe$_2$O$_3$/C and γ-Fe$_2$O$_3$/C@HKUST-1

Samples	BET surface area (m^2 g^{-1})	BJH adsorption average pore width (nm)	BJH desorption average pore width (nm)	Pore volumes (cm^3 g^{-1})
γ-Fe$_2$O$_3$/C	861.6	3.34	3.24	0.57
γ-Fe$_2$O$_3$/C@HKUST-1	993.4	3.32	3.12	0.69

5 It is well known that the surface area is one of the most significant factors that influence the adsorbing capability of adsorbents; thus, high surface areas may lead to an improvement of the adsorbing capability. The pore-size distribution of γ-Fe$_2$O$_3$/C@HKUST-1 and γ-Fe$_2$O$_3$/C was estimated by the BJH 10 method. As shown in Fig. 5, γ-Fe$_2$O$_3$/C has a pore diameter of maxima at 4 nm; the pore diameter of γ-Fe$_2$O$_3$/C@HKUST-1 is smaller than that of γ-Fe$_2$O$_3$/C; however, at ~2 nm another maximum distribution appears, which is related to HKUST-1. This also suggests that the HKUST-1 growing may favor an 15 increase in the surface areas.
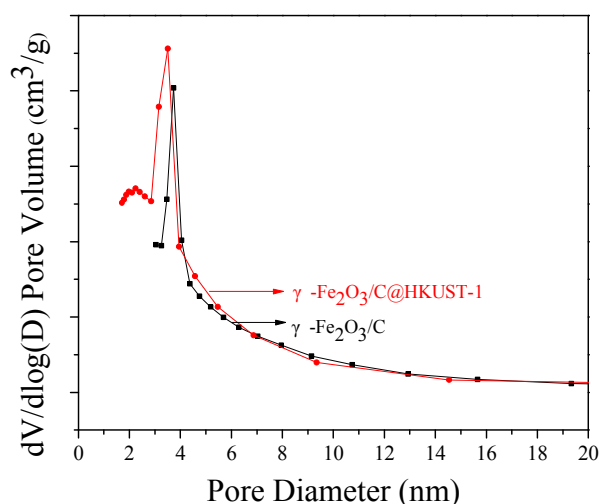
Fig. 5 Pore-diameter distribution of γ-Fe$_2$O$_3$/C@HKUST-1 and γ-Fe$_2$O$_3$/C.

The detailed morphology and microstructure of γ-20 Fe$_2$O$_3$/C@HKUST-1 was characterized by SEM and TEM (shown in Fig. 6 and 7, respectively). Data in Fig. 6a-b clearly suggest that HKUST-1 crystallites are successfully incorporated within the macropores of the γ-Fe$_2$O$_3$/C matrix. In addition, the surface of carbon has amount of ball-like and porous 3D network 25 structures (Fig. 6c and 6d), which play an important role in the adsorption. The TEM images shown in Fig. 7 indicate an ultrafine γ-Fe$_2$O$_3$-particle (~3 nm) uniform distribution in carbon, which is a desirable feature for magnetic separation.
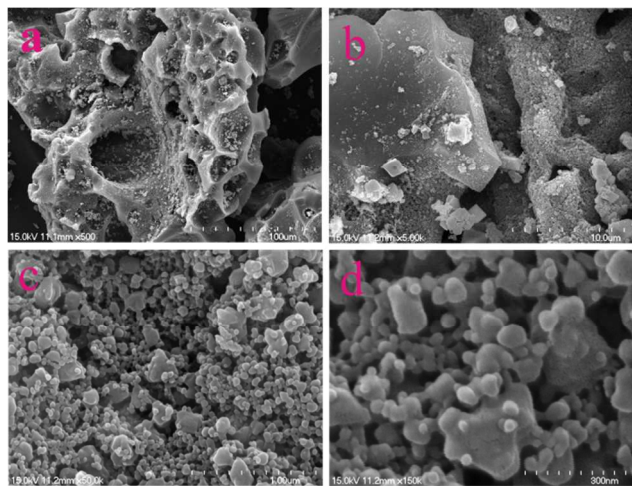
30 **Fig. 6** SEM images of γ-Fe$_2$O$_3$/C@HKUST-1.
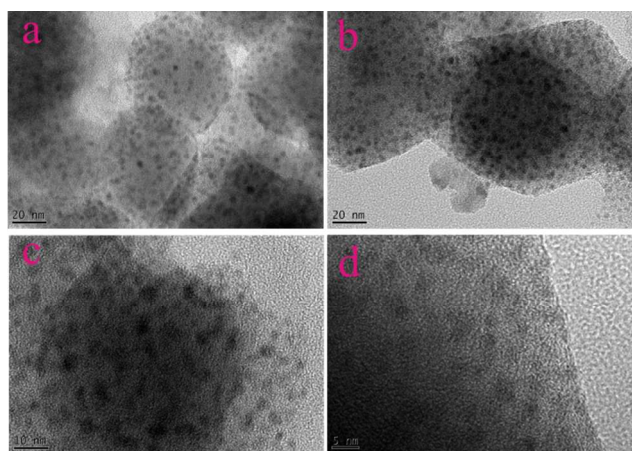
Fig. 7 TEM images of γ-Fe$_2$O$_3$/C@HKUST-1.

The elemental mapping of γ-Fe$_2$O$_3$/C@HKUST-1 revealed the distribution of the four elements within the structures (Fig. 8). In 35 particular, Fe and Cu are uniformly distributed in γ-Fe$_2$O$_3$/C@HKUST-1. Considering the results supported by FT-IR, SEM, TEM and XRD et al, we can conclude that the composite γ-Fe$_2$O$_3$/C@HKUST-1 that consists of γ-Fe$_2$O$_3$/C and HKUST-1 crystallites was successfully synthesized.
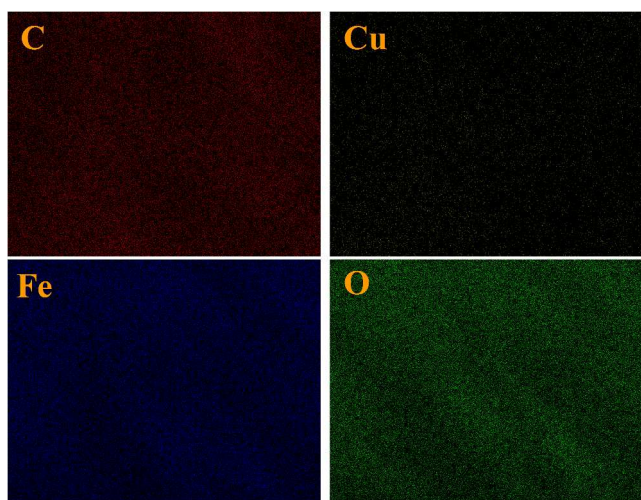
Fig. 8 Elemental mapping of the homogenous dispersion of C, Cu, Fe, and O elements in γ-Fe$_2$O$_3$/C@HKUST-1.

Adsorption of MB and Cr(VI)

5 **Adsorption kinetics**

In order to evaluate the adsorption performance of the prepared γ-Fe$_2$O$_3$/C@HKUST-1 adsorbents, MB and Cr(VI) were employed as pollutant probes for adsorption. As shown in Fig. 9, the adsorption capacity of MB and Cr(VI) significantly increased 10 in the initial 5 h, gradually reaching equilibrium. Moreover, the amount of adsorbed MB and Cr(VI) significantly increased as their initial concentration increased, with a favorable adsorption at high MB and Cr(VI) concentrations. Experimental data were further analyzed in terms of pseudo-second-order kinetic 15 equation:[8]

$$\frac{t}{q_t} = \frac{1}{k_2 q_e^{2}} + \frac{t}{q_e} \qquad (2)$$

where q$_e$ and q$_t$ are the amounts of adsorbate adsorbed on adsorbent (mg g^{-1}) at equilibrium and at a given time t (min), respectively, and k$_2$ the rate constant for pseudo-second-order 20 adsorption (g mg^{-1} min^{-1}). The plots of pseudo-second-order kinetics of MB and Cr(VI) adsorption at different concentrations onto the adsorbent are shown in Fig. S6. The k$_2$ and q$_e$ values were calculated from the intercepts and slopes; These, along with the correlation coefficients (R^2), are listed in Table S1. Data 25 collected in Fig. 9 and Table S1 show that the values obtained from the model fitting also agrees with the experimental data. These results indicate that the overall rate of the adsorption process is controlled by chemisorption.[36]

Adsorption isotherms

30 Adsorption isotherms are usually applied to describe the interaction between the adsorbates and the adsorbents. Fig. 10 shows the adsorption isotherms of MB and Cr(VI) onto γ-Fe$_2$O$_3$/C@HKUST-1, γ-Fe$_2$O$_3$/C, and activated carbon. Our data show that the adsorption capacities sharply increase with the 35 increase in the concentration of adsorbates at equilibrium. Most importantly, the maximum adsorption capacities of γ-

Fe$_2$O$_3$/C@HKUST-1 towards MB and Cr(VI) are 370.2 and 101.4 mg g^{-1}, respectively; these two values are significantly
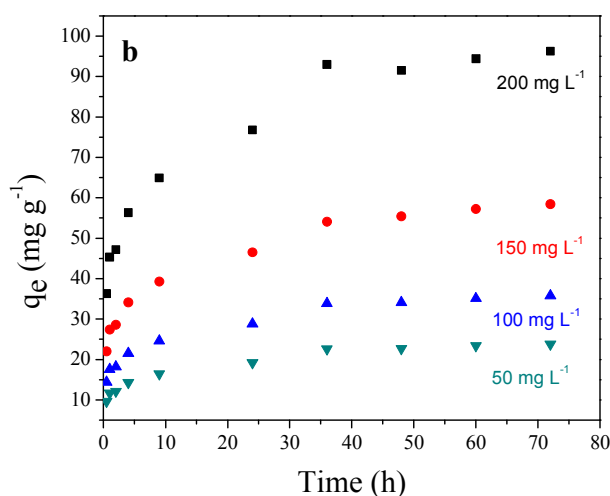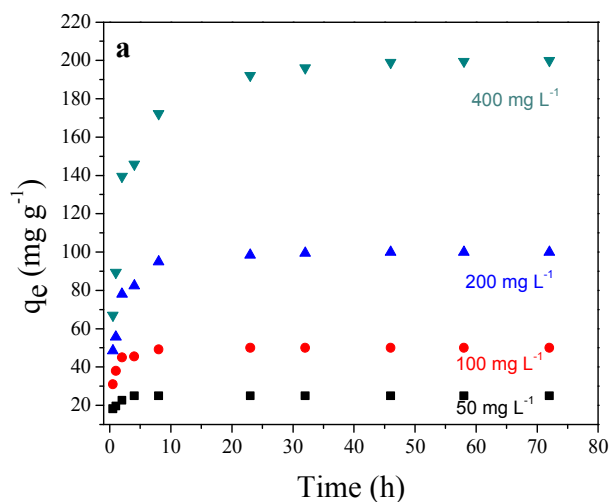
40

Fig. 9 Effects of contact time and initial concentration on the adsorption of MB (a) and Cr(VI) (b) on γ-Fe$_2$O$_3$/C@HKUST-1

higher than those obtained with the other two adsorbents used in these experiments. In addition, the adsorption data were analyzed 45 with the Langmuir equation:[37]

$$\frac{c_e}{q_e} = \frac{c_e}{Q_m} + \frac{1}{Q_m K_L} \qquad (3)$$

where C$_e$ (mg L^{-1}) is the equilibrium concentration, q$_e$ (mg g^{-1}) is the equilibrium adsorption capacity, Q$_m$ (mg g^{-1}) is the maximum adsorption capacity, K$_L$ (L g^{-1}) is the Langmuir constant. Detailed 50 data obtained with this analysis are listed in Table S2; straight lines are obtained when C$_e$/Q$_e$ is plotted against C$_e$, as shown in Fig. S7. In particular, the correlation coefficients R^2 of the Langmuir equation were found to be 0.999 and 0.998 for MB and Cr(VI), respectively, indicating that the adsorption of MB and 55 Cr(VI) perfectly follows the Langmuir adsorption model.

Adsorption thermodynamics

Table 2. Thermodynamic equilibrium constant (K) and relative thermodynamic parameters.

Pollutants	Temperature (K)	K	ΔG (kJ mol^{-1})	ΔH (kJ mol^{-1})	ΔS (J mol^{-1} K^{-1})
MB					
	303	2.5	-2.3		
				28.9	103.1
	323	5.0	-4.3		
Cr (VI)					
	303	2.1	-1.9		
				8.9	35.6
	323	2.6	-2.6		
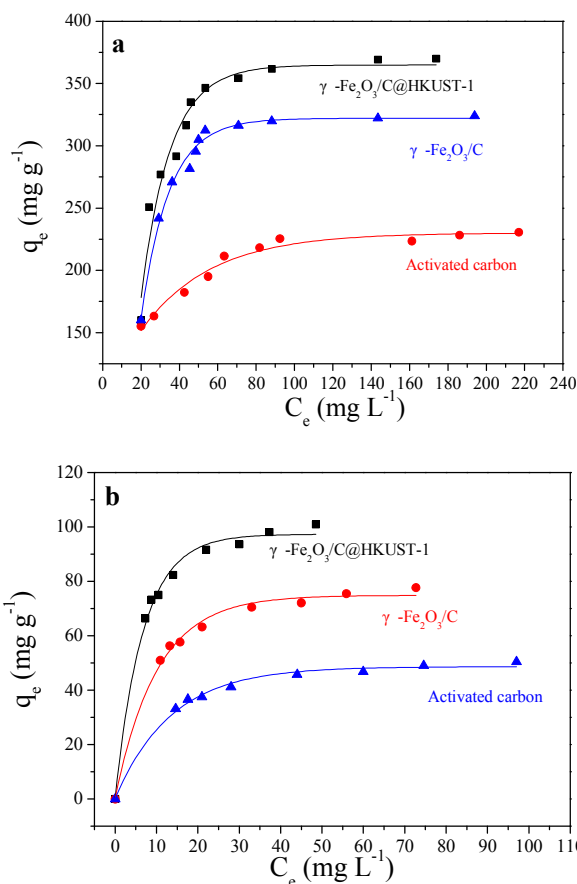
Fig. 10 Adsorption isotherms for MB (a) and Cr(VI) (b) on different adsorbents at 303 K

To determine the effect of temperature on the MB and Cr(VI) adsorption, adsorption experiments were also conducted at 303 and 323 K. The thermodynamic parameters of enthalpy change (ΔH), Gibbs free energy change (ΔG), entropy change (ΔS), and thermodynamic equilibrium constant (K) were computed using the following the equations:[8]

$$K = \frac{q_e}{c_e} \quad (4)$$

$$\Delta G = -RT \ln K \quad (5)$$

$$\ln K = \frac{\Delta S}{R} - \frac{\Delta H}{RT} \quad (6)$$

where K is the adsorption equilibrium constant, q_e the amount of MB or Cr(VI) adsorbed per mass of γ-Fe$_2$O$_3$/C@HKUST-1 (mg g^{-1}), C_e the MB or Cr(VI) concentration in solution at equilibrium (mg L^{-1}), R universal gas constant, and T temperature; results are listed in Table 2. In particular, the positive values of ΔH obtained from this analysis indicate that the adsorption is endothermic, suggesting that the adsorption process is more favorable at higher temperatures. The negative ΔG values are indicative of a spontaneous adsorption; finally, the positive values of ΔS indicate that the adsorption process is irreversible and favors sorption stability.

Effect of pH on sorption of Cr(VI)

It has been proposed that pH is one of the most important parameters that control the Cr(VI) sorption and reduction.[29,38] The effect of pH on the adsorption efficiency can be explained by the surface charge of the adsorbent as well as the metal-ion speciation of the adsorbate. Accordingly, Cr(VI) removal by γ-Fe$_2$O$_3$/C@HKUST-1 was proven to be pH-dependent (Fig. S8); the adsorption capacity at pH 3.0 and 9.0 is the highest and the lowest, respectively, *i.e.*, the increase in pH results in a decrease in Cr(VI) adsorption. The sorption mechanism of surface complexation or bonding is significantly affected by pH, which suggests that the adsorption of Cr(VI) is dominated by surface complexation.[39]

To further explore the effects of pH on the adsorption, based on the experimental data of the total concentration of Cr(VI), we employed Visual MINTEQ 3, a widely used software to simulate equilibria and speciation of inorganic solutes in aqueous solution.[40] The speciation of Cr(VI) under various pH values (Fig. S9) showed that H$_2$CrO$_4$ and HCrO$_4^-$ are the predominant species at pH below 2.0, HCrO$_4^-$ and Cr$_2$O$_7^{2-}$ exist in the pH range of 2.0 to 5.0, and CrO$_4^{2-}$ is the major species at pH above 6.5. At low pH values, γ-Fe$_2$O$_3$ surfaces are protonated, and the net surface charge is positive;[29,41] thus, HCrO$_4^-$ and Cr$_2$O$_7^{2-}$ can be easily sorbed via electrostatic interactions. Furthermore, the unsaturated

metal sites from HKUST-1 could adsorb $Cr_2O_7^{2-}$ by complexation.

The high-resolution XPS spectra of Cr 2p (Fig. S10) showed, upon γ-Fe_2O_3/C@HKUST-1 adsorption of Cr(VI), peaks [5] associated to Cr(III) (Cr 2p$_{1/2}$, 587.0 eV; Cr 2p$_{3/2}$, 577.4 eV), in addition to the characteristic peaks of Cr(VI) (Cr 2p$_{1/2}$, 587.5 eV; Cr 2p$_{3/2}$, 578.6 eV). The ratio of Cr(III)/Cr(VI) on the surface of γ-Fe_2O_3/C@HKUST-1 was found to be 2.2. This suggests that reduction of Cr(VI) to Cr(III) may occur along with the [10] adsorption processes. Cr(VI) has a very high positive redox potential and can be reduced to Cr(III) in the presence of electron donors (*e.g.*, hydroxyl groups) in acidic solution.[42] In addition, the carbon surface of composite may act as suitable substrates for the reduction.[29] This sorption and reduction mechanism may [15] explain the higher Cr(VI) uptake capacity of the γ-Fe_2O_3/C@HKUST-1.

Recycling and reuse

To analyze the recycling and reuse properties of γ-Fe_2O_3/C@HKUST-1 (desirable features of an excellent [20] adsorbent), a reusability test was performed; results are displayed in Fig. 11. Desorption and regeneration of γ-Fe_2O_3/C@HKUST-1 was successfully achieved using acetone and 0.01 M NaOH for MB and Cr(VI), respectively. The removal efficiency at the fifth cycle decreased by about 10% compared to the first adsorption, [25] indicating good regeneration and reusability. Despite this slight decrease, which was attributed to the incomplete desorption of MB and Cr(VI) from the surface of γ-Fe_2O_3/C@HKUST-1, our data confirmed that the magnetic composite proposed in this work can be recycled and reused several times.

[30]
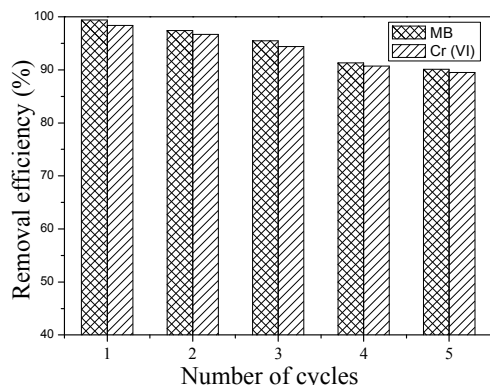
Fig. 11 Regeneration studies of γ-Fe_2O_3/C@HKUST-1 for the removal of MB and Cr(VI)

Conclusions

In summary, we successfully synthesized γ-Fe_2O_3/C [35] incorporated with HKUST-1 by a direct *in situ* crystal growth in a macropore environment. Our results indicated that HKUST-1 plays an important role in increasing the surface area and adsorption capacity. The maximum adsorption capacities of the adsorbents for Cr(VI) and MB are 370.2 and 101.4 mg g^{-1}, [40] respectively; the kinetic adsorption processes fit the pseudo-second-order model, and the isotherms fit the Langmuir model; γ-Fe_2O_3/C@HKUST-1 can be recycled at least 5 times. In addition, the adsorbent γ-Fe_2O_3/C@HKUST-1 promotes the reduction of Cr(VI) to Cr(III) at a low pH. Thus, the data collected in this [45] contribution clearly showed that γ-Fe_2O_3/C@HKUST-1 has a great potential for the adsorption of dyes and heavy metal ions contained in wastewater.

Notes and references

Key Laboratory for the Chemistry and Molecular Engineering of [55] *Medicinal Resources (Ministry of Education of China), College of Chemistry and Pharmaceutical Science of Guangxi Normal University, Guilin 541004, P. R. China.*
Corresponding author: Prof. Fanggui Ye
Tel: +86-773-5856104; fax: +86-773-5832294
[60] ***E-mail address: fangguiye@163.com***

† Electronic Supplementary Information (ESI) available: [details of any supplementary information available should be included here]. See DOI: 10.1039/b000000x/

[65] 1. L. Sun, C. Tian, L. Wang, J. Zou, G. Mu and H. Fu, J Mater Chem, 2011, 21, 7232.
2. Y. Feng, H. Zhou, G. Liu, J. Qiao, J. Wang, H. Lu, L. Yang and Y. Wu, Bioresource Technol, 2012, 125, 138-144.
3. L. Wang, J. Li, Q. Jiang and L. Zhao, Dalton Transactions, 2012, 41, [70] 4544.
4. D. K. Padhi and K. Parida, Journal of Materials Chemistry A, 2014, 2, 10300.
5. J. M. Sun, R. Li and J. C. Huang, Water Sa, 2009, 33.
6. J. H. Chen, H. T. Xing, H. X. Guo, W. Weng, S. R. Hu, S. X. Li, Y. H. [75] Huang, X. Sun and Z. B. Su, Journal of Materials Chemistry A, 2014.
7. X. Liu, L. Yan, W. Yin, L. Zhou, G. Tian, J. Shi, Z. Yang, D. Xiao, Z. Gu and Y. Zhao, Journal of Materials Chemistry A, 2014.
8. S. Huo and X. Yan, J Mater Chem, 2012, 22, 7449.
9. J. Wang, G. Zhao, Y. Li, H. Zhu, X. Peng and X. Gao, Dalton [80] Transactions, 2014, 43, 11637.
10. Y. Jiang, X. Yu, T. Luo, Y. Jia, J. Liu and X. Huang, Journal of Chemical & Engineering Data, 2013, 58, 3142-3149.
11. R. L. Liu, Y. Liu, X. Y. Zhou, Z. Q. Zhang, J. Zhang and F. Q. Dang, Bioresour Technol, 2014, 154, 138-147.
[85] 12. P. K. Tripathi, M. Liu, Y. Zhao, X. Ma, L. Gan, O. Noonan and C. Yu, Journal of Materials Chemistry A, 2014, 2, 8534.
13. M. Wawrzkiewicz, Chem Eng J, 2013, 217, 414-425.
14. J. Cao, J. Li, L. Liu, A. Xie, S. Li, L. Qiu, Y. Yuan and Y. Shen, Journal of Materials Chemistry A, 2014, 2, 7953.
[90] 15. S. M. Jung, H. Y. Jung, W. Fang, M. S. Dresselhaus and J. Kong, Nano Lett, 2014, 14, 1810-1817.
16. P. K. Tripathi, L. Gan, M. Liu and N. N. Rao, J Nanosci Nanotechno, 2014, 14, 1823-1837.
17. S. Zhang, M. Zeng, J. Li, J. Li, J. Xu and X. Wang, Journal of [95] Materials Chemistry A, 2014, 2, 4391.
18. H. J. Lee, W. Cho, E. Lim and M. Oh, Chem Commun, 2014, 50, 5476.
19. X. Zhu, Y. Liu, C. Zhou, S. Zhang and J. Chen, ACS Sustainable Chemistry & Engineering, 2014, 2, 969-977.
[100] 20. L. Zhou, Y. Shao, J. Liu, Z. Ye, H. Zhang, J. Ma, Y. Jia, W. Gao and Y. Li, ACS Applied Materials & Interfaces, 2014, 6, 7275-7285.
21. N. L. Torad, M. Hu, S. Ishihara, H. Sukegawa, A. A. Belik, M. Imura, K. Ariga, Y. Sakka and Y. Yamauchi, Small, 2014, 10, 2096-2107.
22. N. A. Khan, Z. Hasan and S. H. Jhung, J Hazard Mater, 2013, 244-[105] 245, 444-456.
23. L. Li, X. L. Liu, H. Y. Geng, B. Hu, G. W. Song and Z. S. Xu, Journal of Materials Chemistry A, 2013, 1, 10292.

24. D. Qian, C. Lei, G. Hao, W. Li and A. Lu, ACS Applied Materials & Interfaces, 2012, 4, 6125-6132.

25. P. B. Somayajulu Rallapalli, M. C. Raj, D. V. Patil, K. P. Prasanth, R. S. Somani and H. C. Bajaj, Int J Energ Res, 2013, 37, 746-753.

5 26. L. Li, X. L. Liu, M. Gao, W. Hong, G. Z. Liu, L. Fan, B. Hu, Q. H. Xia, L. Liu, G. W. Song and Z. S. Xu, Journal of Materials Chemistry A, 2014, 2, 1795.

27. M. E. Silvestre, M. Franzreb, P. G. Weidler, O. Shekhah and C. Wöll, Adv Funct Mater, 2013, 23, 1210-1213.

10 28. D. J. Tranchemontagne, J. R. Hunt and O. M. Yaghi, Tetrahedron, 2008, 64, 8553-8557.

29. M. Baikousi, A. B. Bourlinos, A. Douvalis, T. Bakas, D. F. Anagnostopoulos, J. Tuček, K. Šafářová, R. Zboril and M. A. Karakassides, Langmuir, 2012, 28, 3918-3930.

15 30. N. Anand, K. H. P. Reddy, T. Satyanarayana, K. S. R. Rao and D. R. Burri, Catalysis Science & Technology, 2012, 2, 570.

31. J. Xiao, L. Qiu, X. Jiang, Y. Zhu, S. Ye and X. Jiang, Carbon, 2013, 59, 372-382.32. Y. Liu, L. Yu, Y. Hu, C. Guo, F. Zhang and X. Wen David Lou, Nanoscale, 2011, 4, 183.

20 32. Y. Liu, L. Yu, Y. Hu, C. Guo, F. Zhang and X. Wen David Lou, Nanoscale, 2011, 4, 183.

33. X. Zhu, Y. Liu, F. Qian, C. Zhou, S. Zhang and J. Chen, Bioresource Technol, 2014, 154, 209-214.

34. Z. Zhong, J. Yao, Z. Low, R. Chen, M. He and H. Wang, Carbon, 25 2014, 72, 242-249.

35. S. S. Chui, S. M. Lo, J. P. Charmant, A. G. Orpen and I. D. Williams, Science, 1999, 283, 1148-1150.

36. R. Liu, Y. Liu, X. Zhou, Z. Zhang, J. Zhang and F. Dang, Bioresource Technol, 2014, 154, 138-147.

30 37. X. Zhao, D. Liu, H. Huang, W. Zhang, Q. Yang and C. Zhong, Micropor Mesopor Mat, 2014, 185, 72-78.

38. A. Idris, E. Misran, N. Hassan, A. A. Jalil and C. E. Seng, J Hazard Mater, 2012, 227-228, 309-316.

39. Y. Li, S. Zhu, Q. Liu, Z. Chen, J. Gu, C. Zhu, T. Lu, D. Zhang and J. 35 Ma, Water Res, 2013, 47, 4188-4197.

40. H. Shen, J. Chen, H. Dai, L. Wang, M. Hu and Q. Xia, Ind Eng Chem Res, 2013, 52, 12723-12732.

41. P. Wang and I. M. C. Lo, Water Res, 2009, 43, 3727-3734.

42. Y. Jiang, X. Yu, T. Luo, Y. Jia, J. Liu and X. Huang, Journal of 40 Chemical & Engineering Data, 2013, 58, 3142-3149.

RSC Advances Accepted Manuscript